Article

Generation of polarization-sensitive modulated optical vortices with all-dielectric metasurfaces

Chao Yan, Xiong Li, Mingbo Pu, Xiaoliang Ma, Fei Zhang, Ping Gao, Yinghui Guo, Kaipeng Liu, Zuojun Zhang, and Xiangang Luo

ACS Photonics, **Just Accepted Manuscript** • DOI: 10.1021/acsphotonics.8b01119 • Publication Date (Web): 04 Jan 2019

is published by the American Chemical Society. 1155 Sixteenth Street N.W., Washington, DC 20036

Article type: Full Paper

Title: Generation of polarization-sensitive modulated optical vortices with all-dielectric metasurfaces

Chao Yan, [†,‡,§] Xiong Li, [†,‡,§] Mingbo Pu, [†,‡] Xiaoliang Ma, [†,‡] Fei Zhang, [†] Ping Gao , [†] Yinghui Guo , [†] Kaipeng Liu, [†] Zuojun Zhang, [†] and Xiangang Luo*[,†,‡]

[†]State Key Laboratory of Optical Technologies on Nano-Fabrication and Micro-Engineering, Institute of Optics and Electronics, Chinese Academy of Sciences, P. O. Box 350, Chengdu 610209, China
[‡]University of Chinese Academy of Sciences, Beijing 100049, China
§These authors contributed equally.
* Corresponding Author: lxg@ioe.ac.cn

ABSTRACT

Optical vortices (OVs) created from helical modes of light have extensive applications in optical manipulation, imaging and optical communications. Moreover, modulated optical vortices (MOVs) with modified wavefronts could provide new opportunities for fractionating particles and actuating microelectromechanical systems. Traditional devices for generating MOVs include spatial light modulators, spiral phase plates etc. However, such bulky devices are difficult to be applied to high-level integrated optical systems. Besides, other MOV generators are typically static and polarization-insensitive. Here, we proposed an all-dielectric metasurface to generate polarization-sensitive MOVs. The intensity patterns of the OVs can be modulated by adding a tangential modulation factor in the phase profile. Independent manipulation of two orthogonal polarizations was adopted via tailoring the geometric parameters of silicon (Si) pillars. We experimentally demonstrated that the metasurface could generate a doughnut and an actinomorphic vortex beams for different polarization inputs. In

addition, the intensity pattern of the MOVs can be dynamically tuned by adjusting the polarization angle. This work can benefit optical manipulation and can be further extended to visible and near-infrared bands.

KEYWORDS: all-dielectric metasurfaces, modulated optical vortices, polarizations, mid-infrared, propagation phase

An optical vortex (OV) is characterized by a helical phase factor of $exp(il\theta)$, where l is the topological charge and θ the azimuth angle in the plane normal to optical axis. This phase factor converts the plane wave into a helix winding around the optical axis. It was proved that each photon in a vortex beam carries orbital angular momentum （OAM） of $l\hbar$. [1-5] Typically, the core of an OV is dark and the beam's intensity is distributed to an annulus. OVs have extensive applications in optical manipulation, [6-7] imaging [8-9] and optical communications. [10-11] Moreover, the intensity patterns of an OV can be modulated with an irregular-shaped spiral phase plate, [12] a deformable mirror [13] or a spatial light modulator (SLM), etc. [14-16] For instance, SLMs are widely used to generate MOVs via phase profile modulation. This generalized class of OVs may exhibit novel properties, offering applicable tools for optical manipulation in mesoscopic systems. [6,14] However, these devices for generation of MOVs are normally bulky, which is difficult to be applied to high-level integrated optical systems. In contrast, recently a new platform based on metasurfaces was proposed to generate MOVs in a much integrated way with high design flexibility. [5,17,18]

A metasurface is an artificial subwavelength planar array to control the propagation of electromagnetic (EM) waves, which provides a valuable platform for ultrathin and planar optics.[18-26] The meta-atoms of metasurfaces can be engineered to shift phase and amplitude, thus realizing functions such as polarization testing,[22] Fano resonances,[23] and superoscillations.[24,25] Particularly, one could design the meta-atoms to impart different phase profiles on orthogonal polarizations.[18,27] Thus a metasurface consisting of these meta-atoms can fulfill different functions depending on the polarization of incident light. Such metasurfaces have been achieved with plasmonic antennas[19,28] and dielectric posts fabricated on Si,[29-32] TiO_2,[18] GaAs,[33] SiN,[34] or GaN.[35] Owing to the designed flexibility at the subwavelength scale, metasurfaces can also be used to generate vortex beams. The generation of optical vortices and the associated functionalities including multiplexing can be achieved by both plasmonic and dielectric metasurfaces.[36-40] Besides, optical vortices can also be generated and controlled by making use of the scattering and dissipation of metallic nanoparticles.[41,42] Compared with the traditional devices, the metasurface-based OV generators combine the virtues of miniaturization, easy design and fabrication, revealing great potentials for generating complex vortex beams.

In this work, we employ the propagation phase to design a metasurface operating at a wavelength of 10.6 μm. The phase shift imposed by the metasurface to the x and y-polarized waves are respectively denoted as ϕ_x and ϕ_y. For each unit cell, ϕ_x and ϕ_y can be tailored by changing its size while its angular orientation remains fixed. This allows for the imposition of distinct OVs on orthogonal linear polarization states. As a proof of concept, we modify the intensity patterns of the OVs by adding a tangential modulation factor in the phase profile. This modulated phase profile can generate an actinomorphic intensity pattern. In experiment, the generated OVs can be switched from a closed shape to an open one by adjusting the polarization of the incident light. This work exhibits the merits of an ultrathin, polarization-sensitive MOV generator with easy design and fabrication. These advantages may suggest potential applications in optical manipulation and communication of optical metasurfaces.

PRINCIPLE AND DESIGN

The proposed metasurface generates and focuses MOVs via phase profile modulation. The total phase profile φ can be described as a superimposition of two parts

$$\varphi = \varphi_1 + \varphi_2, \tag{1}$$

where φ_1 is responsible for generating two different MOVs to the x and y-polarized light and φ_2 is used for focusing the generated MOVs. For φ_1, one can construct different expressions based on the helical phase factor. For instance, we can choose

$$\varphi_1(\theta) = l[\theta + \alpha \tan(m\theta + \beta)], \tag{2}$$

where θ is the azimuth angle in the plane of device normal to optical axis , l is topological charge and m is a positive integer. Compared with the conventional helical phase profile, an extra tangential modulation factor is added in this formula. This phase profile is expected to produce a $2m$-fold symmetric OV whose size depends on α and whose orientation is controlled by β. We set the center of the plane of the device as the reference point. To confine an OV to a smaller area, a converging phase profile φ_2 is superimposed on the modulated helical phase, which can be written as

$$\varphi_2(r) = \frac{2\pi}{\lambda}(\sqrt{r^2 + f^2} - f), \tag{3}$$

where λ=10.6 μm is the designed wavelength; $r = \sqrt{x^2 + y^2}$ is the distance from an arbitrary point $R(x, y)$ on the plane of the device to the reference point and f is the focal length.

The pattern of the MOV at the focal plane can be described by [14]

$$R(\theta) = a\frac{\lambda}{NA}\left[1 + \frac{1}{l_0}\frac{d\varphi(\theta)}{d\theta}\right], \tag{4}$$

where $R(\theta)$ is the local radius of maximum intensity at azimuth angle θ, NA is the sample's numerical aperture, $\varphi(\theta)$ is the phase modulation described by Equation (1) and the constants a and l_0 depend on the beam's radial amplitude profile. Inserting Equation (1) into Equation (4), we can obtain

$$R(\theta) = a\frac{\lambda}{NA}\left[1 + \frac{1}{l_0}(1 + \mathrm{m}\,\alpha(\sec^2(\mathrm{m}\,\theta + \beta)))\right]. \tag{5}$$

The predicted radial profile with $l = 15$, $m = 3$ and $\alpha = 1$ is displayed in **Figure 1**a. It shows that the predicted profile agrees well with the simulated intensity pattern obtained with the phase modulation described by Equation (1). For $m = 3$, the actinomorphic pattern is 6-fold symmetric. To further prove that the intensity pattern is $2m$ -fold symmetric, Figure S1 depicts the simulated intensity patterns obtained by changing m with fixed α and by changing α with fixed m. It is also shown that increasing m and α can enlarge the intensity patterns.

The schematic illustration of the proposed metasurface for monochromatic light is shown in **Figure 2**a. In this illustration, the metasurface is composed of square pixels. The dimension of each pixel is smaller than wavelength to avoid diffraction of light into high diffraction orders. The metasurface consists of a single layer of Si rectangular pillars with different dimensions. The pillars are positioned at the centers of square unit cells. Each pillar can be considered as a waveguide which functions as a Fabry-Pérot resonator with low quality factor. [30] The whole Si layer is constructed on a Si substrate. The rectangular cross sections of the pillars result in different effective indices of waveguide modes polarized along x and y-axis. Consequently, each pillar imposes a polarization dependent phase shift to the transmitted wave. Light is primarily confined in the high refractive index pillars acting as weakly coupled resonators. The light scattered by the pillars is mainly influenced by the geometrical parameters of the pillars and has negligible reliance on sizes of the adjacent pillars. It is shown in Figure 2 that the edges of each pillar are parallel to the x or y-axis. Thus a normally incident wave which is linearly polarized along the x or y-axis does not alter its polarization and only obtains phase and amplitude modulation as it traverses the array.

The transmitted phases ϕ_x and ϕ_y are dependent on the pillar side length l_x and l_y. Therefore, the array act as a device with modifiable birefringence and its principal axes are along x and y directions. The desired phases (ϕ_x and ϕ_y) are selected via varying the side length of the pillars. The height of the pillars h and the lattice constant p are fixed when we select the suitable parameters l_x and l_y, where h=10 μm and p=4.7 μm, respectively.

In principle, arbitrary phase modulation can be realized by changing the parameters of the proposed unit cell. To demonstrate this capability without loss of generality, we adopt an eight-level phase modulation with 45° interval to cover the whole 360° phase shift. For independent phase control of two orthogonal polarizations, a complete set of eight-level phase response thus requires 8×8 types of unit cell (8×8 groups of l_x and l_y).

To obtain the 64 types of unit cell, numerical simulations were performed using commercial software CST Microwave Studio. The simulations were operated at mid-infrared wavelength of 10.6 μm (28.3 THz). The 10 μm high Si pillar (with refractive index of 3.42 at 10.6 μm) rests on a Si substrate. Unit cell boundary conditions are applied in both the x and y directions and Floquet-port excitation is set in the z direction. The incident light is linearly polarized along the x- (or y-) axis, and scattering parameters of the transmitted x (or y)-polarized electric field are then calculated. Therefore the phase shift imposed by a unit cell to the transmitted x and y-polarized waves (i.e. ϕ_x and ϕ_y) are obtained. Due to symmetry, once the values of l_x and l_y are interchanged, the corresponding ϕ_x and ϕ_y interchange accordingly. As a result, the actual number of types required to use is 36.

RESULTS AND DISCUSSION

The overall transmitted phase profiles for the 64 types of unit cell are presented in **Figure 3**a. Each point in Figure 3a represents a combination of ϕ_x and ϕ_y. These combinations of ϕ_x and ϕ_y are obtained by selecting geometrical parameters l_x and l_y from the simulations mentioned above. In consideration of fabrication, we computed these phases and amplitude transmission coefficients for all values of l_x and l_y in the range 1 μm to 3.7 μm. For most unit cells, the amplitude transmission coefficients are more than 0.7. The transmission efficiency at the mid-infrared band can be further improved by assigning different materials for pillars and substrate. [43]

Figure 3b depicts the magnetic energy density distribution in an array of Si pillars resting on the Si substrate under plane wave incidence. The optical energy is confined inside the pillars, leading to weak coupling among the pillars. Thus, the phase modulation by the Si rectangular pillars can be considered as a local effect in this case. We chose two typical structures and obtained their wavelength dependence of amplitude transmission coefficients and the corresponding unwrapped transmitted phase for the x and y-polarized inputs, as shown in Figure 3c. The operation wavelength (10.6 μm) we chose avoids the resonances. It is also demonstrated in Figure 3c that $l_x = l_y$ leads to $\phi_x = \phi_y$ and $t_x = t_y$.

To demonstrate the performance of MOV generation, we designed and fabricated three samples operating at the mid-infrared wavelength of 10.6 μm, as shown in **Figure 4**a. Each of them generates two different OVs for two orthogonal incident polarizations via phase modulation φ described by Equation (3). We measured the generated intensity patterns at focal plane (f =1.86 cm) using the experiment setup displayed in Figure 4b.

As presented in Figure 4a, an actinomorphic and a doughnut shaped vortex beams are produced by the x and y-polarized light, respectively. These OVs are modulated by choosing different parameters in Equation (1). Compared with the conventional OV, the MOVs with actinomorphic pattern may offer new features for particle manipulation. Just as the normal OVs exert torques on particles, the MOVs can also exert tangential forces. Particles tend to move more or less uniformly around a conventional OV, [9] whereas a modulated OV can drive them through complicated trajectories. [6,14] This combination of OVs could be applied to distinguish and manipulate particles according to their shape and size. When a linear-polarized beam with polarization angle of 45° illuminates on the metasurface, the combined OVs can be observed. Moreover, any desired combinations of OVs can be realized using our devices through selection of phase modulation. The designed intensity patterns should be perfectly centrosymmetric, as shown in simulation results in Figure 1b. However, the experimental results in Figure 4a show that some areas in a pattern are more intense than other areas. This discrepancy could be attributed to the ununiform laser spot and the fabrication errors, as well as to the imperfect normal incidence.

Furthermore, the doughnut shaped pattern can be gradually transformed into the actinomorphic one by changing the polarization angle of incident light, as illustrated in Figure S2. The experimental results agree well with simulations, which is consistent with our design goals. It should be noted that different phase modulations lead to varied relative intensities of the two OVs at the same polarization angle. Although the metasurface can simultaneously create two OVs at most, the proposed design approach can be readily applied for multiple OVs generation using multi-channel approaches [37] or shared-aperture array techniques. [44]

The proposed approach for generating OVs offers several advantages. First, the intensity of patterns can be controlled by polarization angle of incident linear-polarized light. Our platform provides a new tool for dynamic control of vortex light generation in comparison with conventional generators. It should be noted that the design method can be extended to other EM spectrums although the experiment was performed at the mid-infrared wavelength. Besides, combining with the shared-aperture array or multi-channel techniques, a single device can generate multiple polarization-controlled MOVs simultaneously. This improves the capacity of optical communication and enhances the ability of optical manipulation.

METHODS

The designed patterns were fabricated via direct laser writing in the photoresist coated on a double-side polished Si wafer (approximately 1.94 mm thick). Following this, the patterns of photoresist were transferred into Si wafer using inductive-coupled plasmonic (ICP) etching to form Si pillars. The SEM images of three samples are depicted in Figure 4a.

Figure 4b shows the schematic illustration of the measurement setup that was employed to characterize the designed MOV generators. A mid-infrared CO_2 laser tunable from 9.3 μm to 10.7 μm was utilized as the illumination source. After passing through an adjustable attenuator, the optical beam was sent through a beam expander, followed by a linear polarizer and an aperture, and then transmitted to the sample from substrate. The transmitted intensity patterns were recorded by an infrared CCD (384 × 288 pixels, UA330, Guide-Infrared Inc.) at focal plane. The size of each pixel was 25 μm × 25 μm.

CONCLUSION

In this paper, we have demonstrated an all-silicon metasurface to realize the generation of polarization-controlled MOVs at mid-infrared range. An eight-level phase modulation with 45° interval was used to independently control the transmitted phase for both the x and y polarizations. Sixty-four types of unit cell were designed via tailoring and optimizing the geometric parameters of Si pillars. It is shown that a single metasurface can create two distinct OVs with a doughnut and an actinomorphic intensity patterns for the x and y polarization input, respectively. Besides, by adjusting the polarization angle, the intensity pattern of the MOV composed of these two OVs can be tuned. This performance improves the dynamic control capability of OV generation. In addition, the all-silicon metasurface was fabricated with one-step laser direct writing followed by a single etching process. In contrast to conventional OV generators, our design based on the all-dielectric metasurface combines the virtues of miniaturization, easy design and fabrication. Compared with other devices generating MOVs, the proposed metasurface may promote the miniaturization and integration of the optical systems utilizing vortex generators.

ASSOCIATED CONTENT

Supporting Information

Simulation results of MOVs under varied parameters, simulation and experiment results under varied polarization angle. Supporting Information is available from the Wiley Online Library or from the author.

AUTHOR INFORMATION

Corresponding Author

*E-mail: lxg@ioe.ac.cn

Notes

The authors declare no competing financial interest.

ACKNOWLEDGMENTS

This work is supported by the National Natural Science Funds of China under Contact No. 61675207, 61822511 and 61705234.

REFERENCES

(1) Allen, L.; Beijersbergen, M. W.; Spreeuw, R. J.; Woerdman, J. P. Orbital angular momentum of light and the transformation of Laguerre-Gaussian laser modes. *Phys. Rev. A* **1992**, *45*, 8185.

(2) Allen, L.; Barnett, S. M.; Padgett, M. J. *Optical angular momentum*; Institute of Physics Publishing, Bristol, 2003.

(3) He, H.; Friese, M. E.; Heckenberg, N. R.; Rubinszteindunlop, H. Direct observation of transfer of angular momentum to absorptive particles from a laser beam with a phase singularity. *Phys. Rev. Lett.* **1995**, *75*, 826.

(4) O'Neil, A. T.; Macvicar, I.; Allen, L.; Padgett, M. J. Intrinsic and extrinsic nature of the orbital angular momentum of a light beam. *Phys. Rev. Lett.* **2002**, *88*, 053601.

(5) Pu, M.; Li, X.; Ma, X.; Wang, Y.; Zhao, Z.; Wang, C.; Hu, C.; Gao, P.; Huang, C.; Ren, H. Catenary optics for achromatic generation of perfect optical angular momentum. *Sci. Adv.* **2015**, *1*, e1500396.

(6) Grier, D. G. A revolution in optical manipulation. *Nature* **2003**, *424*, 810.

(7) Gao, D.; Ding, W.; Nieto-Vesperinas, M.; Ding, X.; Rahman, M.; Zhang, T.;

Lim, C.; Qiu, C. W. Optical manipulation from the microscale to the nanoscale: fundamentals, advances and prospects. *Light: Sci. Appl.* **2017**, *6*, e17039.

(8) Franke-Arnold, S.; Allen, L.; Padgett, M. Advances in optical angular momentum. *Laser Photonics Rev.* **2010**, *2*, 299.

(9) Yao, A. M.; Padgett, M. J. Orbital angular momentum: origins, behavior and applications. *Adv. Opt. Photonics* **2011**, *3*, 161.

(10) Wang, J.; Yang, J. Y.; Fazal, I. M.; Ahmed, N.; Yan, Y.; Huang, H.; Ren, Y.; Yue, Y.; Dolinar, S.; Tur, M. Terabit free-space data transmission employing orbital angular momentum multiplexing. *Nat. Photonics* **2012**, *6*, 488.

(11) Willner, A. E.; Molisch, A. F.; Bao, C.; Xie, G.; Huang, H.; Wang, J.; Li, L.; Tur, M.; Lavery, M. P. J.; Ahmed, N. Optical communications using orbital angular momentum beams. *Adv. Opt. Photonics* **2015**, *7*, 66.

(12) Lee, W. M.; Yuan, X. C.; Cheong, W. C. Optical vortex beam shaping by use of highly efficient irregular spiral phase plates for optical micromanipulation. *Opt. Lett.* **2004**, *29*, 1796.

(13) Tyson, R. K.; Scipioni, M.; Gbur, G. Production and propagation of a modulated optical vortex through atmospheric turbulence. *Proceed. SPIE* **2009,** *7200*, 72000G.

(14) Curtis, J. E.; Grier, D. G. Modulated optical vortices. *Opt. Lett.* **2003**, *28*, 872.

(15) Tseng, S. Y.; Hsu, L. Controlling the transverse momentum distribution of a light field via azimuth division of a hologram in holographic optical tweezers. *Appl. Opt.* **2011**, *50*, 62.

(16) Cho, S. W.; Kim, H.; Hahn, J.; Lee, B. Generation of multiple vortex-cones by direct-phase modulation of annular aperture array. *Appl. Opt.* **2012**, *51*, 7295.

(17) Hong, M. Metasurface wave in planar nano-photonics. *Sci. Bull*. **2016**, *61*, 112-113

(18) Balthasar Mueller, J. P.; Rubin, N. A.; Devlin, R. C.; Groever, B.; Capasso, F. Metasurface polarization optics: independent phase control of arbitrary orthogonal states of polarization. *Phys. Rev. Lett.* **2017**, *118*, 113901.

(19) Yu, N.; Genevet, P.; Kats, M. A.; Aieta, F.; Tetienne, J. P.; Capasso, F.; Gaburro, Z. Light propagation with phase discontinuities reflection and refraction. *Science* **2011**, *334*, 333.

(20) Luo, X. Principles of electromagnetic waves in metasurfaces. *Sci. China Phys. Mech. Astron.* **2015**, *58*, 594201.

(21) Pu, M.; Ma, X.; Li, X.; Guo, Y.; Luo, X. Merging plasmonics and metamaterials by two-dimensional subwavelength structures. *J. Mater. Chem. C* **2017**, *5*, 4361.

(22) Kruk, S.; Hopkins, B.; Kravchenko, I. I.; Miroshnichenko, A.; Neshev, D. N.; Kivshar, Y. S. Broadband highly efficient dielectric metadevices for polarization control. *APL Photonics* **2016**, *1*, 030801.

(23) Luk'yanchuk, B. S.; Miroshnichenko, A. E.; Yu, S. K. Fano resonances and topological optics: an interplay of far- and near-field interference phenomena. *J. Opt.* **2013**, *15*, 073001.

(24) Berry, M. V.; Moiseyev, N. Superoscillations and supershifts in phase space: Wigner and Husimi function interpretations. *J. Phys. A: Math. Theor.* **2014**, *47*,

315203.

(25) Yuan, G. H., Rogers, E. T.; Zheludev, N. I. 'Plasmonics' in free space: observation of giant wavevectors, vortices and energy backflow in superoscillatory optical fields. 2018, arXiv:physics/1805.11794v1. arXiv.org e-Print archive. https://arxiv.org/abs/1805.11794v1 (accessed May 30, 2018).

(26) Zhang, M.; Pu, M.; Zhang, F.; Guo, Y.; He, Q.; Ma, X.; Huang, Y.; Li, X.; Yu, H.; Luo, X. Plasmonic metasurfaces for switchable photonic spin-orbit interactions based on phase change materials. *Adv. Sci.* **2018**, *5*, 1800835.

(27) Zhang, F.; Pu, M.; Yu, H.; Luo, X. Symmetry breaking of photonic spin-orbit interactions in metasurfaces. *Opto-Electron. Eng.* **2017**, *44*, 319.

(28) Li, X.; Chen, L.; Li, Y.; Zhang, X.; Pu, M.; Zhao, Z.; Ma, X.; Wang, Y.; Hong, M.; Luo, X. Multicolor 3D meta-holography by broadband plasmonic modulation. *Sci. Adv.* **2016**, *2*, e1601102.

(29) Lin, D.; Fan, P.; Hasman, E.; Brongersma, M. L. Dielectric gradient metasurface optical elements. *Science* **2014**, *345*, 298.

(30) Arbabi, A.; Horie, Y.; Bagheri, M.; Faraon, A. Dielectric metasurfaces for complete control of phase and polarization with subwavelength spatial resolution and high transmission. *Nat. Nanotechnol.* **2015**, *10*, 937.

(31) Yang, Y.; Wang, W.; Moitra, P.; Kravchenko, I. I.; Briggs, D. P.; Valentine, J. Dielectric meta-reflectarray for broadband linear polarization conversion and optical vortex generation. *Nano Lett.* **2014**, *14*, 1394.

(32) Zhang, F.; Pu, M.; Li, X.; Gao, P.; Ma, X.; Luo, J.; Yu, H.; Luo, X. All-dielectric

metasurfaces for simultaneous giant circular asymmetric transmission and wavefront shaping based on asymmetric photonic spin-orbit interactions. *Adv. Funct. Mater.* **2017**, *27*,1704295

(33) Hasman, E.; Kleiner, V.; Bomzon, Z. E. Pancharatnam–Berry phase in space-variant polarization-state manipulations with subwavelength gratings. *Opt. Lett.* **2001**, *26*, 1424.

(34) Colburn, S; Zhan, A.; Bayati, E.; Whitehead, J.; Ryou, A.; Huang, L.; Majumdar, A. Broadband transparent and CMOS-compatible flat optics with silicon nitride metasurfaces. *Opt. Mater. Express* **2018**, *8*, 2330-2344.

(35) Chen, B. H.; Wu, P. C.; Su, V.-C.; Lai, Y.-C.; Chu, C. H.; Lee, I. C.; Chen, J.-W.; Chen, Y. H.; Lan, Y.-C.; Kuan, C.-H.; Tsai, D. P. GaN Metalens for pixel-level full-color routing at visible light. *Nano Lett.* **2017**, *17*, 6345-6352.

(36) Li, Y.; Li, X.; Chen, L.; Pu, M.; Jin, J.; Hong, M.; Luo, X. Orbital angular momentum multiplexing and demultiplexing by a single metasurface. *Adv. Opt.Mater.* **2017,** *5*, 1600502.

(37) Jin, J.; Pu, M.; Wang, Y.; Li, X.; Ma, X.; Luo, J.; Zhao, Z.; Gao, P.; Luo, X. Multi-channel vortex beam generation by simultaneous amplitude and phase modulation with two-dimensional metamaterial. *Adv. Mater. Technol.* **2017**, *2*, 1600201.

(38) Luo, X. Subwavelength artificial structures: opening a new era for engineering optics. *Adv. Mater.* **2018**, DOI: 10.1002/adma.201804680.

(39) Nemati, A.; Wang, Q.; Hong, M.; Teng, J. Tunable and reconfigurable

metasurfaces and metadevices. *Opto-Electron. Adv.* **2018**, *1*, 180009.

(40) Luo, X.; Tsai, D.; Gu, M.; Hong, M. Subwavelength interference of light on structured surfaces. *Adv. Opt. Photonics* **2018**, *10*, 757-842.

(41) Wang, Z. B.; Luk'yanchuk, B. S.; Hong, M. H.; Lin, Y.; Chong, T. C. Energy flow around a small particle investigated by classical Mie theory. *Phys. Rev. B* **2004**, *70*, 035418.

(42) Bashevoy, M. V.; Fedotov, V. A.; Zheludev, N. I. Optical whirlpool on an absorbing metallic nanoparticle. *Opt. Express* **2005**, *13*, 8372-8379.

(43) Zhang, F.; Yu, H.; Fang, J.; Zhang, M.; Chen, S.; Wang, J.; He, A.; Chen, J. Efficient generation and tight focusing of radially polarized beam from linearly polarized beam with all-dielectric metasurface. *Opt. Express* **2016**, *24*, 6656.

(44) Maguid, E.; Yulevich, I.; Veksler, D.; Kleiner, V.; Brongersma, M. L.; Hasman, E. Photonic spin-controlled multifunctional shared-aperture antenna array. *Science* **2016**, *352*, 1202.

FIGURES

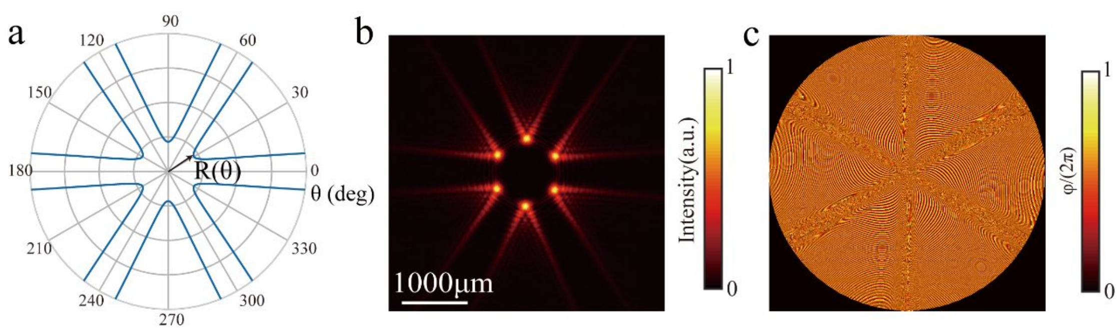

Figure 1. A MOV with *l*=15, *m*=3 and *α*=1. (a) Theoretical radial profile *R(θ)*. (b) Simulated intensity profile at focal plane. c) Phase profile of the designed metasurface.

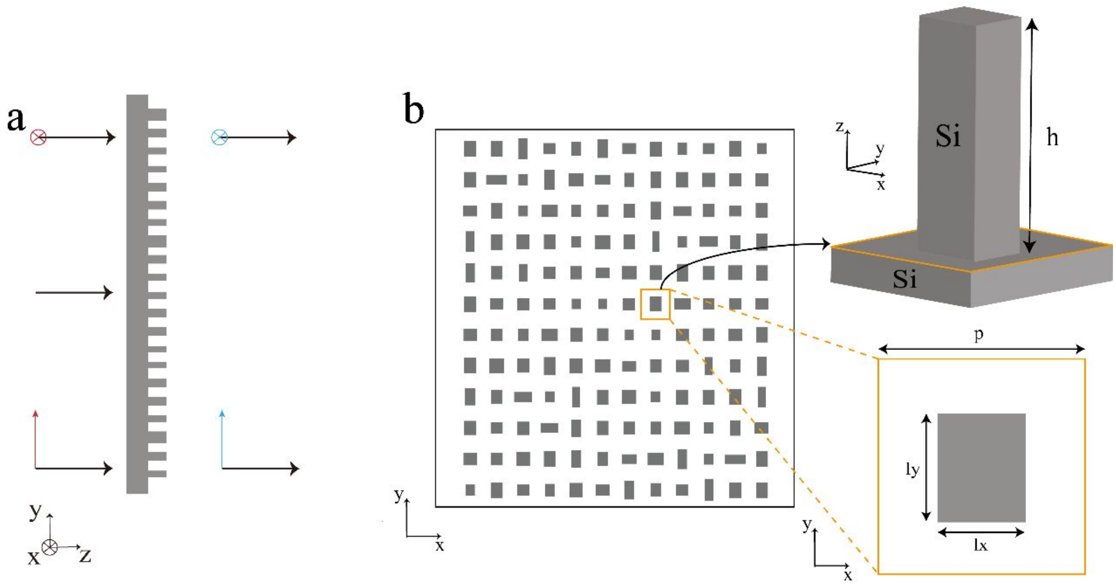

Figure 2. Illustration of the designed metasurface for generation of MOVs. (a) Schematic side view of the proposed metasurface. Each element (inset of Figure 2b) imparts unique phase ϕ_x and ϕ_y on two orthogonal, linearly polarized input light (red, on left). The element dimensions can be varied to adjust the imposed phase while the orientation angle remain fixed. The polarization states of output (blue, on right) are unconverted. (b) Top view of the designed metasurface. The metasurface is composed of rectangular Si pillars with identical height (10 μm) and period (4.7 μm), different side length (l_x and l_y) which are positioned at the centers of square pixels. The insets show a 3D schematic of a unit cell and magnified top view.

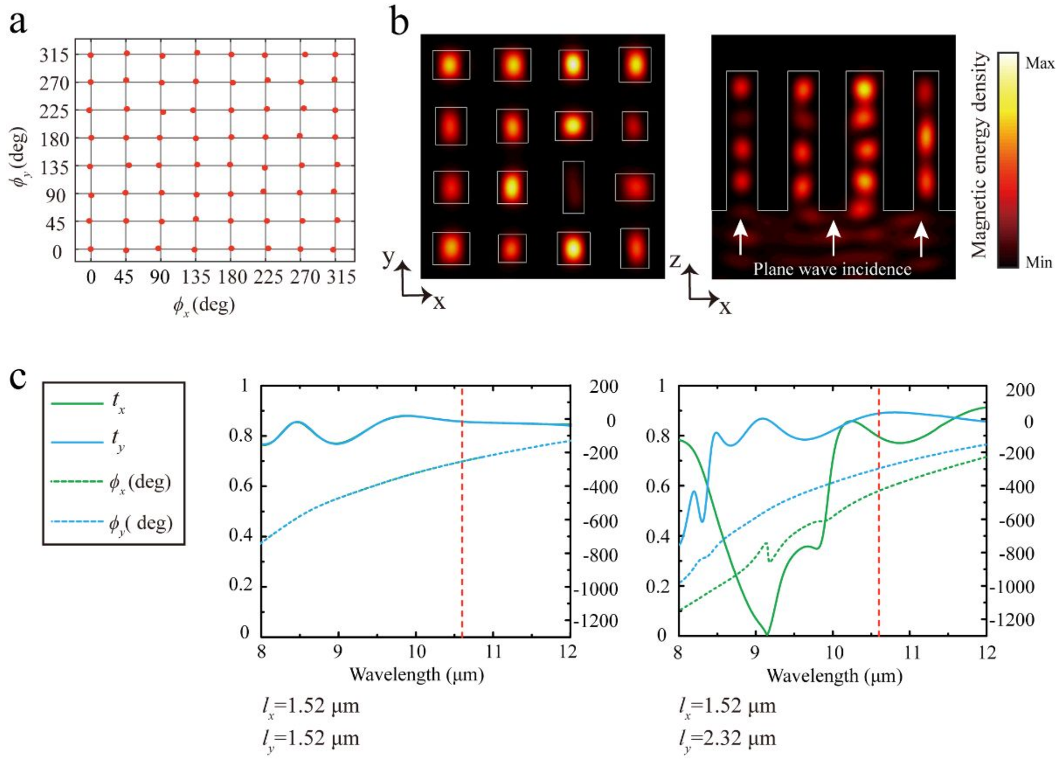

Figure 3. (a) Simulated color coded values of the amplitude transmission coefficients of optimized unit cells. For independent phase control of two orthogonal polarizations (ϕ_x for x-polarization and ϕ_y for y-polarization), a complete set of eight-level transmitted phase response with 45° interval is adopted to cover the whole 360° modulation. Each of the 8×8 points corresponds to a specific set of structural parameters. (b) Simulated magnetic energy density distribution of an array of Si pillars with Si substrate under plane wave incidence. The white lines show the edges of the pillars. (c) Wavelength dependence of amplitude transmission coefficients (t_x and t_y) and the corresponding unwrapped transmitted phase for periodic arrays of the desired Si pillars under x and y-polarized incidences. The spectras are shown for two (l_x, l_y) combinations: (1.52 μm, 1.52 μm), (1.52 μm, 2.32 μm). The desired operation wavelength (10.6 μm) is depicted with dashed red vertical lines, which does not overlap with any resonances of the arrays.

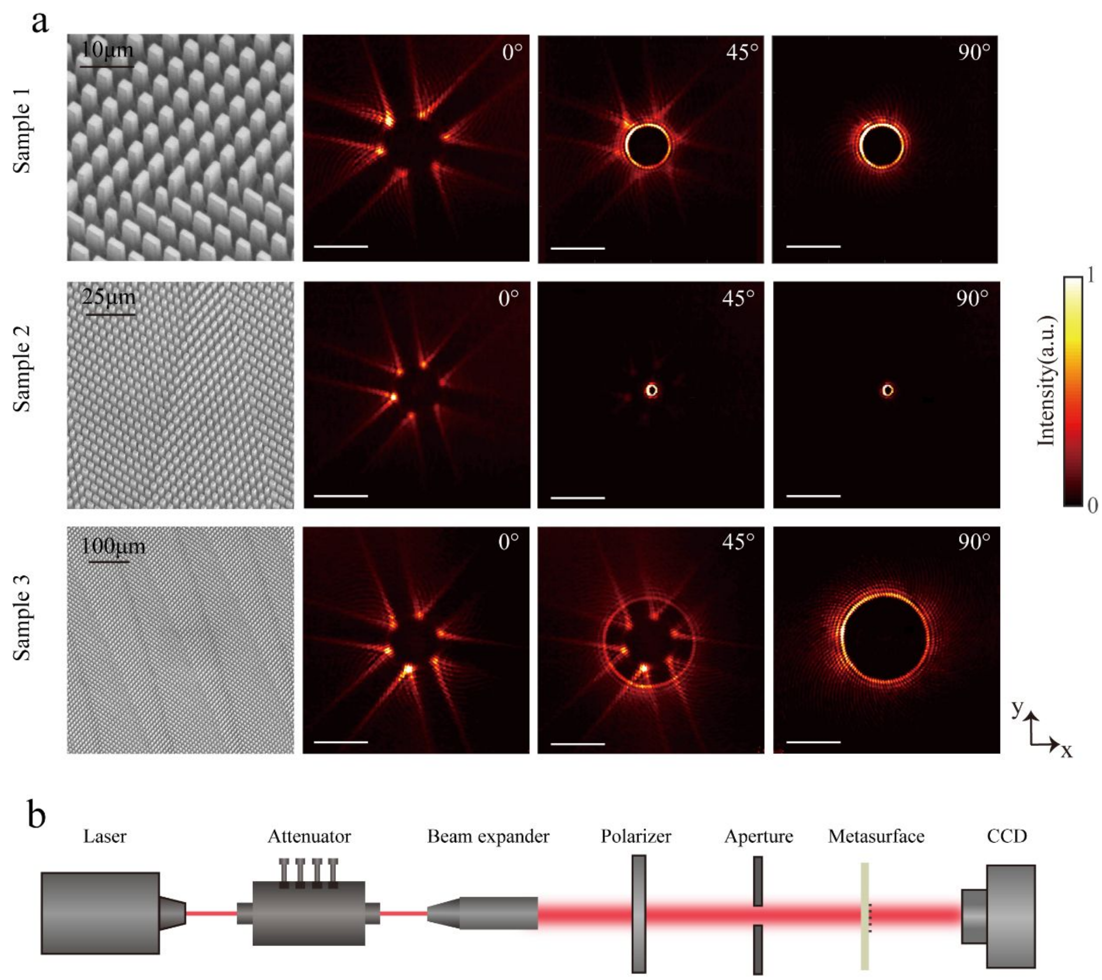

Figure 4. (a) Measured results for three samples. Each row shows intensity profiles of the OVs at focal plane under linear-polarized incidence with polarization angle of 0° (x-polarization), 45° and 90° (y-polarization), accompanied by the SEM images of the three samples. For the design wavelength of 10.6μm, the focal length is 1.86 cm. Sample 1 generates two OVs with l=15, α=1, m=3 and l=45, α=0 for the x and y-polarized light, respectively. Sample 2 generates two OVs with l=15, α=1, m=3 and l=10, α=0 for the x and y-polarized light, respectively. Sample 3 generates two OVs with l=15, α=0.8, m=3 and l=100, α=0 for the x and y-polarized light, respectively. White scale bars indicate 1000 μm. (b) Schematic illustration of the measurement setup.

For Table of Contents Use Only

Title: Generation of polarization-sensitive modulated optical vortices with all-dielectric metasurfaces

Chao Yan, [†,‡,§] Xiong Li, [†,‡,§] Mingbo Pu, [†,‡] Xiaoliang Ma, [†,‡] Fei Zhang, [†] Ping Gao , [†] Yinghui Guo , [†] Kaipeng Liu, [†] Zuojun Zhang, [†] and Xiangang Luo*,[†,‡]

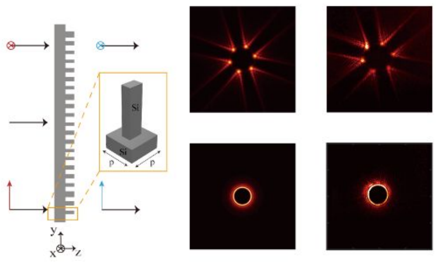

An all-silicon metasurface was designed to generate polarization-sensitive modulated optical vortices (MOVs). We experimentally demonstrated that the metasurface could generate a doughnut and an actinomorphic vortex beams for different polarization input. The generated optical vortices can be switched from a closed shape to an open one by adjusting the polarization of the incident light. Compared with previously proposed metasurface-based MOV generators and conventional bulk optical elements, this work exhibits the merits of an ultrathin, polarization-sensitive MOV generator with easy design and fabrication. Besides, combining with the shared-aperture array or multi-channel techniques, a single device can generate multiple polarization-controlled MOVs simultaneously. These advantages may suggest potential applications in optical manipulation and communication of optical metasurfaces.

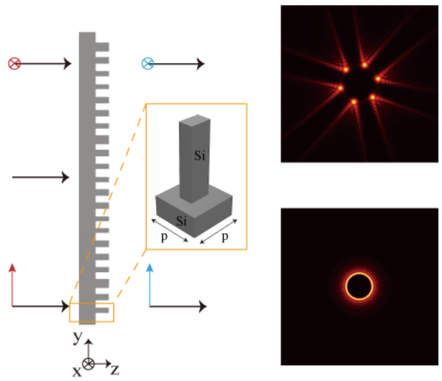

An all-silicon metasurface was designed to generate polarization-sensitive modulated optical vortices (MOVs). We experimentally demonstrated that the metasurface could generate a doughnut and an actinomorphic vortex beams for different polarization input. The generated optical vortices can be switched from a closed shape to an open one by adjusting the polarization of the incident light. Compared with previously proposed metasurface-based MOV generators and conventional bulk optical elements, this work exhibits the merits of an ultrathin, polarization-sensitive MOV generator with easy design and fabrication. Besides, combining with the shared-aperture array or multi-channel techniques, a single device can generate multiple polarization-controlled MOVs simultaneously. These advantages may suggest potential applications in optical manipulation and communication of optical metasurfaces.

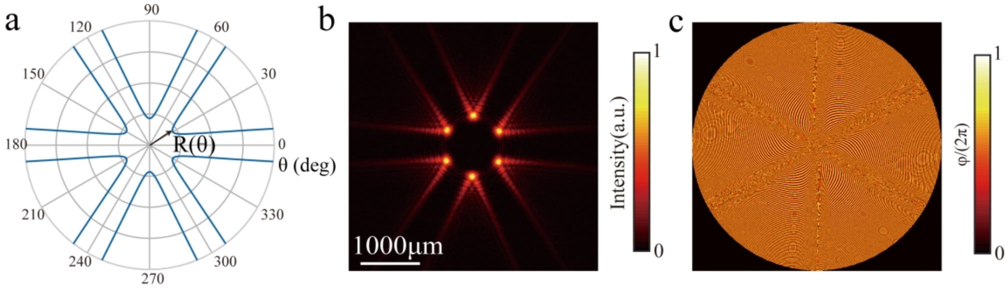
a
90
60
30
0
330
300
270
240
210
180
150
120
R(θ)
θ (deg)
b
1000μm
Intensity(a.u.)
1
0
c
φ/(2π)
1
0

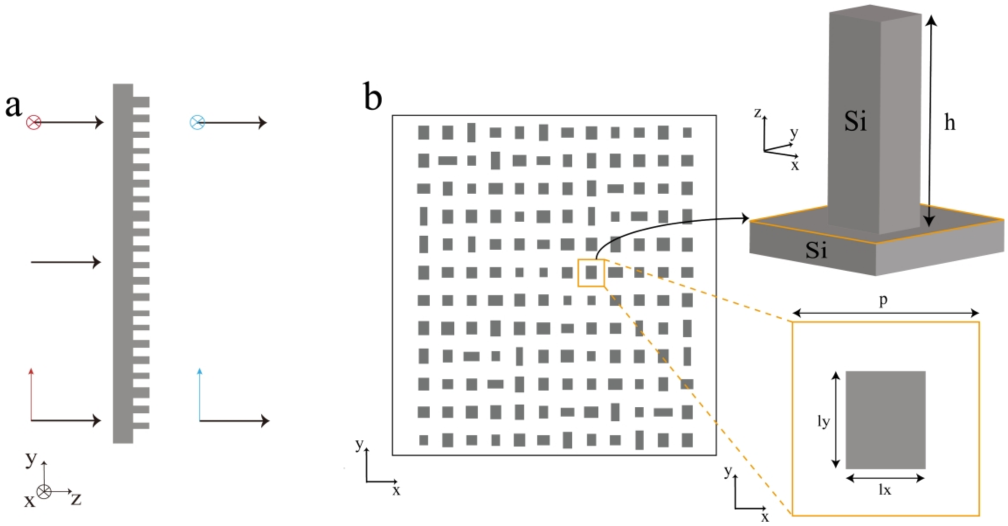
a
y
x
z
b
y
x
z
y
x
Si
h
Si
p
ly
lx
y
x

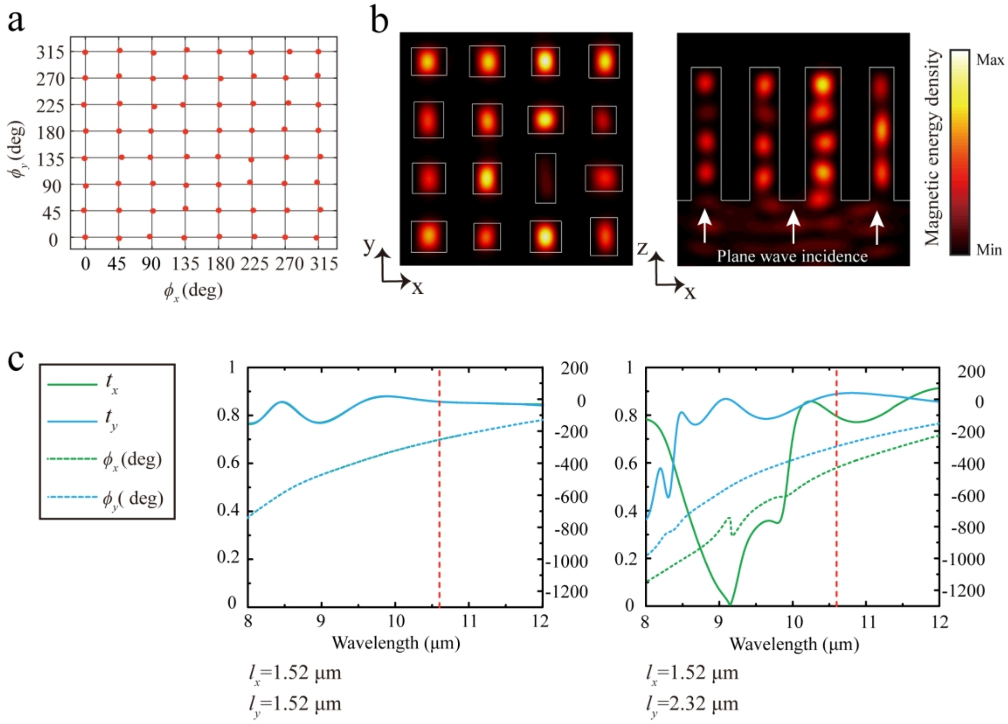
a
b
c
ϕ_y (deg)
ϕ_x (deg)
Plane wave incidence
Magnetic energy density
Max
Min
t_x
t_y
ϕ_x (deg)
ϕ_y(deg)
Wavelength (μm)
l_x=1.52 μm
l_y=1.52 μm
l_x=1.52 μm
l_y=2.32 μm

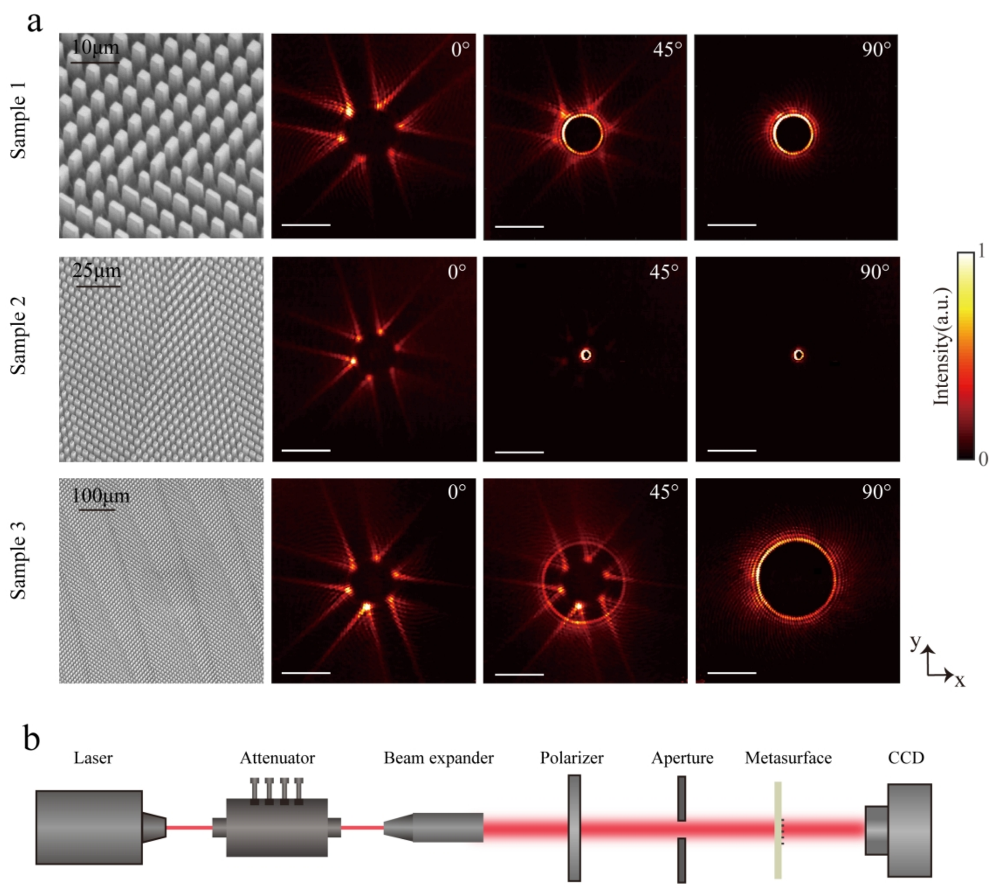

199x179mm (300 x 300 DPI)